 doi:10.20944/preprints202203.0354.v1

Article

Synthesis, Computational and Nanoencapsulation Studies on Eugenol-Derived Insecticides

Catarina M. M. Coelho[a], Renato B. Pereira[b], Tatiana F. Vieira[c,d], Cláudia M. Teixeira[a,b], Maria José G. Fernandes[a], Ana Rita O. Rodrigues[e,f], David M. Pereira[b], Sérgio F. Sousa[c,d], A. Gil Fortes[a], Elisabete M. S. Castanheira[e] and M. Sameiro T. Gonçalves[a,*]

[a] Centre of Chemistry, Department of Chemistry, University of Minho, Campus of Gualtar, 4710-057 Braga, Portugal;
[b] REQUIMTE/LAQV, Laboratory of Pharmacognosy, Department of Chemistry, Faculty of Pharmacy, University of Porto, R. Jorge Viterbo Ferreira, 228, 4050-313 Porto, Portugal;
[c] UCIBIO/REQUIMTE, BioSIM – Departamento de Medicina, Faculdade de Medicina da Universidade Do Porto, Alameda Prof. Hernâni Monteiro, 4200-319 Porto, Portugal;
[d] Associate Laboratory i4HB - Institute for Health and Bioeconomy, Faculdade de Medicina, Universidade do Porto, 4200-319 Porto, Portugal;
[e] Physics Centre of Minho and Porto Universities (CF-UM-UP), University of Minho, Campus of Gualtar, 4710-057 Braga, Portugal;
[f] Associate Laboratory LaPMET - Laboratory of Physics for Materials and Emergent Technologies, University of Minho, Campus of Gualtar, 4710-057 Braga, Portugal.
* Correspondence: msameiro@quimica.uminho.pt

Abstract: A new set of alkoxy alcohols were synthesised by reaction of eugenol oxirane with aliphatic and aromatic alcohols. These eugenol derivatives were evaluated against their effect upon the viability of the insect cell line *Sf9* (*Spodoptera frugiperda*). The most promising compounds, 4-(3-(*tert*-butoxy)-2-hydroxypropyl)-2-methoxyphenol and 4-(2-((4-fluorobenzyl)oxy)-3-hydroxypropyl)-2-methoxyphenol were submitted to *in silico* assays to predict possible targets. Throught an Inverted Virtual Screening approach, 23 common pesticide targets were screened and the top 2 targets predicted were further analyzed through molecular dynamics simulations and free energy calculations. In addition, these eugenol derivatives were subjected to encapsulation and release assays using liposome-based nanosystems of egg phosphatidylcholine/cholesterol (7:3), with encapsulation efficiencies higher than 90% and release profiles well described by both Korsmeyer-Peppas and Weibull models.

Keywords: insecticides; semi-synthetic pesticides; eugenol derivatives; alkoxy alcohols; essential oils; nanoencapsulation biopesticides;

1. Introduction

Food production and human health are greatly affected by insects. One way to control pests is the resource to synthetic insecticides. Despite being used frequently, the inappropriate utilization of these compounds is related to the development of resistance to pests, human diseases and contamination of food and environment. Consequently, the biological action of natural products with insecticidal activity is a very important alternative that allows the management, in an environmental-friendly way, the action of insects and pests, without affecting people's health [1-3]. There has been a growing interest in studying and evaluating the action of botanical insecticides for pest management due to insect resistance to the traditional insecticides [2-4].

Essential oils (EOs), a complex natural mixtures of secondary plant metabolites, have interesting insecticidal biological properties, being effective against several diseases or pests, frequently with low to none negative impact to the environment and non-targeted organisms [5,6]. They present a broad spectrum of activity against insect pests and plant pathogenic fungi, including insecticidal, antifeedant, repellent, oviposition deterrent,

 doi:10.20944/preprints202203.0354.v1

growth regulatory, and antivector activities [7-9]. Some examples of compounds found in EOs with insecticidal activity are linalool, thymol, eugenol, α-terpineol, carvacrol, limonene, α-pinene, citronellol, geraniol, citral and 1,8-cineole [3, 10,11].

Eugenol is the major component of *Syzygium aromaticum* (clove) oil (70-90%). The biological properties associated with eugenol are highly varied [12], including promising antimicrobial, antioxidant and insecticide properties [13].

The broad spectrum of biological activity makes eugenol, 4-allyl-2-methoxy phenol, a target molecule for structural modifications to produce compounds with higher biological activity [14]. Structural modifications from 4-allyl-2-methoxy phenol can be carried out on the hydroxyl group and the double bond [15], and some of the derivatives were reported as new potential botanical insecticides [16], being effective on a wide variety of domestic arthropod pests [14,17]. Several studies have demonstrated that a structural modification of some EOs' constituents can increase the biocidal effect of these phytochemicals, increasing their insecticidal activity [18,19].

Eugenol epoxide can be an important intermediate to produce eugenol derivatives. With the ring-opening reaction of eugenol epoxide with nucleophiles like alcohols, it is possible to synthetize β-alkoxy alcohols, which have tremendous applications as intermediates in pharmaceuticals. The versatility of β-alkoxy alcohols allow them to participate in the synthesis of many organic compounds, in making a wide range of unnatural amino acids, biologically active and synthetic [20-21].

The synthesis of β-alkoxy alcohol is one of the important reactions due to its wider application in the synthesis of potent insecticidal penifulvins bicyclic backbones and for the direct synthesis of α-alkoxy ketones [22-23]. β-Amino alcohols are important organic compounds of considerable use in medicinal chemistry, amino acids, and chiral auxiliaries [24].

Taking these facts into consideration and our ongoing research [25-26] where some eugenol derivatives revealed high potential as semi-synthetic pesticides, in the present work a completely new series of eugenol alkoxy alcohols derivatives were obtained, and their insecticidal activity evaluated against the *Sf9* (*Spodoptera frugiperda*) insect cell line.

Considering its insecticidal activity, the most promising compounds, 4-(3-(*tert*-butoxy)-2-hydroxypropyl)-2-methoxyphenol and 4-(2-((4-fluorobenzyl)oxy)-3-hydroxypropyl)-2-methoxyphenol, were submitted to *in silico* assays to predict possible targets. Throught an Inverted Virtual Screening approach, 23 common pesticide targets were screened. The top 2 targets predicted were further analyzed through molecular dynamics simulations and free energy calculations, to validate the docking predicitons and estimate binding free energies of association.

In addition, these to eugenol derivatives were subjected to nanoencapsulation and release studies using liposome-based nanosystems of egg-yolk phosphatidylcholine/cholesterol (Egg-PC:Ch) (7:3). This formulation is environmentally friendly, biodegradable and stable in physiological conditions, with no concerns related to toxicity, even being used to prepare suitable models of biomembranes.

2. Results and Discussion

2.1. Chemistry

The synthesis involved in the present work started by reaction of 4-allyl-2-methoxyphenol **1**, commonly known as eugenol, with *m*-chloroperoxybenzoic acid, in dichloromethane, to afford 2-methoxy-4-(oxiran-2-ylmethyl)phenol **2** [26]. In order to obtain a new set of eugenol **1** alkoxy alcohols having varied structures possessing alkyl linear or non-linear chains of different sizes, a triple bond, phenyl rings, and halogens atoms, compound **2** was reacted with a selected series of aliphatic and aromatic alcohols, in the presence of a Lewis acid.

Thus, under nitrogen atmosphere, at low temperature, using boron trifluoride diethyl etherate, 2-methoxy-4-(oxiran-2-ylmethyl)phenol **2** was reacted with methanol,

Preprints (www.preprints.org) | NOT PEER-REVIEWED | Posted: 28 March 2022 doi:10.20944/preprints202203.0354.v1

ethanol, *tert*-butanol, phenol, 3-butyn-2-ol, 3-bromopropan-1-ol or 4-fluorobenzyl alcohol, to give the corresponding eugenol alkoxy alcohols derivatives, namely 4-(2-hydroxy-3-methoxypropyl)-2-methoxyphenol **3a**, 4-(3-ethoxy-2-hydroxypropyl)-2-methoxyphenol **3b**, 4-(3-(*tert*-butoxy)-2-hydroxypropyl)-2-methoxyphenol **3c**, 4-(2-hydroxy-3-phenoxy-propyl)-2-methoxyphenol **3d**, 4-(2-(but-3-yn-2-yloxy)-3-hydroxypropyl)-2-methoxyphenol **3e**, 4-(2-(3-bromopropoxy)-3-hydroxypropyl)-2-methoxyphenol **3f** and 4-(2-((4-fluorobenzyl)oxy)-3-hydroxypropyl)-2-methoxyphenol **3g**, respectively (Scheme 1). These compounds were obtained as oils or a solid material (**3b**) in 8 to 68% yields, and were fully characterized by IR, ^{1}H and ^{13}C NMR spectroscopy and HRMS. The ^{1}H NMR spectra suggest that the oxirane ring opening reaction with the first four alcohols occurred by nucleophilic attack on the less substituted carbon (primary carbon), probably via the S_N2 mechanism with the loss of a leaving group (ring-opening) to occur at the same time, resulting in compounds **3a-d**. On the other hand, in the remaining three alcohols, the nucleophilic attack seems to occur at the most substituted carbon (secondary carbon) of the oxirane, which is consistent with the S_N1 mechanism, resulting in compounds **3e-g**. In the ^{1}H NMR spectra stand out the presence of the signals of protons CHOH as multiplets (δ 4.55– 3.89 ppm) for compounds **3a-d**, while for compounds **3e-g** are visible the signals of protons CHO to lower deviations also as multiplets (δ 3.88–3.42 ppm). The presence of signals of the methylene group directly attached to the terminal OH appeared as multiplets (δ 3.73–3.42 ppm) for compounds **3e-g**.

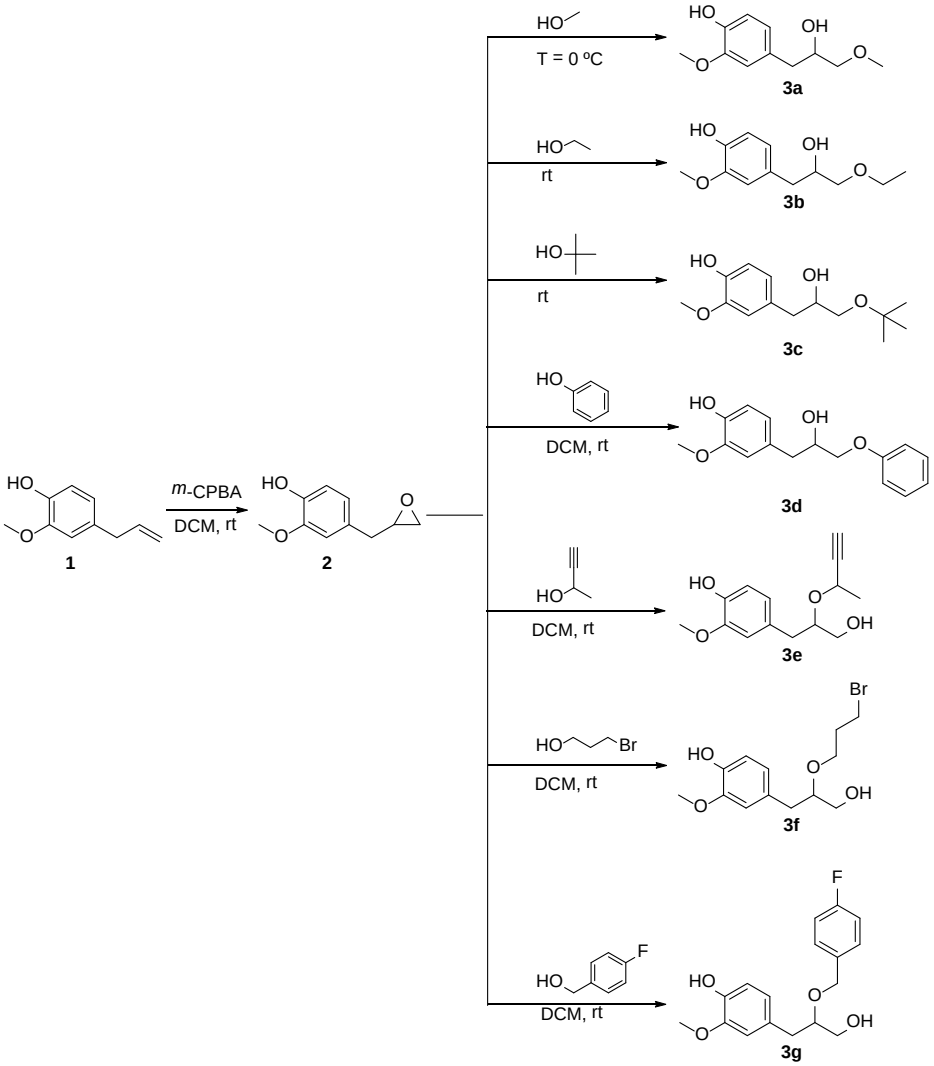

Scheme 1. Synthesis of compounds 3a-g.

Preprints (www.preprints.org) | NOT PEER-REVIEWED | Posted: 28 March 2022 doi:10.20944/preprints202203.0354.v1

In the ^{13}C NMR spectra, the confirmation of epoxide opening was verified by the presence of different signals for C*H*OH or CHO groups emerging for compounds **3a-d** (δ 79.63-71.37 ppm) and **3e-g** (δ 81.62-80.33 ppm), respectively, and methylene carbons of CH_2OH group (δ 64.54 – 63.67 ppm) for compounds **3e-g**.

In addition, for compounds **3a-g**, the ^{1}H and ^{13}C NMR spectra also showed the different characteristic signals for the aromatic protons (δ 7.32-6.70 ppm) and carbons (δ 146.46-111.30 ppm), respectively. The IR spectra of compounds **3a-g** displayed stretching bands characteristics of the hydroxyl groups between 3381 and 3425 cm^{-1}.

2.2. Biological evaluation of alkoxy alcohols 3a-g

The study of the insecticidal activity of the synthesized compounds **3a-g** was carried out in two-dimensional (2D) cultures of *Sf9* cells, which are derived from ovary cells of *Spodoptera frugiperda*. For comparison purposes, all the molecules were tested at the same concentration (100 μg/mL) (Figure 1). Compounds **3e** and **3f**, containing a substituted hydroxyl group in the side chain, displayed low toxicity towards *Sf9* cells causing *ca.* 20% viability loss, similar to the starting materials, eugenol **1** and eugenol epoxide **2**. On the other hand, the reaction of eugenol epoxide **2** with methanol, ethanol and phenol afforded three β-alkoxy alcohols completely devoid of toxicity (**3a**, **3b**, and **3d** respectively). Among all eugenol-derived alkoxy alcohols synthesized (**3a-g**), **3c** and **3g** showed increased toxicity, when compared with **1** and **2** (Figure 1). Compound **3c**, whose structure includes a non-linear alkyl chain with three terminal methyl groups, was the second most active molecule, causing *ca.* 25% viability loss. Remarkably, compound **3g**, whose structure includes a group of methanol derivative in which one of the H atoms of the methyl group was replaced by fluorophenyl, was the most active, eliciting *ca.* 40% viability loss. Noteworthy, both molecules (**3c** and **3g**) presented equal or even higher toxicity than the commercial insecticide, chlorpyrifos (CHPY) [26], being selected therefore for nanoencapsulation studies.

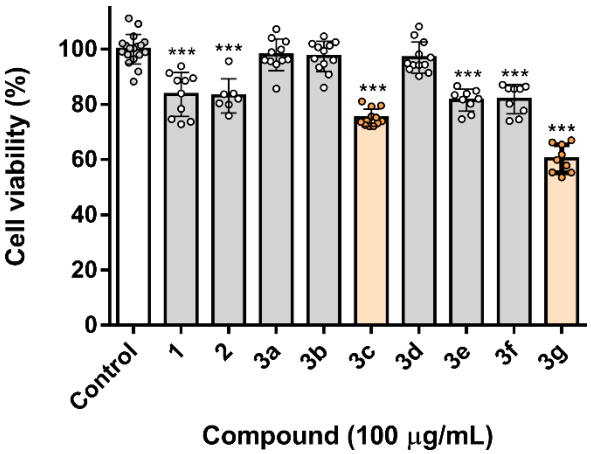

Figure 1. Viability of the *Sf9* cells after incubation with the presented molecules (100 μg/mL), or medium (control). Cells were incubated for 24 h, after which viability was evaluated. *** $p < 0.001$.

2.3. Inverted virtual screening results

Depicted in Table 1 are the average scores obtained for compounds **3c** and **3g** in complex with the list of possible targets, for each scoring function studied. The different scoring functions are based on different metrics and scales, hence, the difference in the range of values. The GOLD scoring functions are dimensionless and the interpretation of the score is the following: a more positive value signifies a better binding affinity. AutoDock Vina, on the other hand, uses a system of measurement that is a more real approximation of the binding free energy, indicating that a more negative score signifies better affinity.

 doi:10.20944/preprints202203.0354.v1

The predictions of all the different SF were ranked from best to worst and the PDB structure that presented the best score was selected as potential target. Considering the results obtained, compounds 3c and **3g** showed increased affinity toward odorant binding protein 1 (OBP) and acetylcholinesterase (AChE). The same tendency was observed throughout all the SF tested.

Table 1. Average scores of the amino alcohol derivatives of eugenol **3c** and **3g** obtained for all PDB structures with the five different scoring functions and overall ranking of the most likely protein targets for interaction.

Target	PDB	PLP	ASP	ChemScore	GoldScore	Vina	Overall ranking
Acetylcholinesterase	1QON	84.71	55.80	36.09	64.74	-8.25	2
	1DX4	77.59	48.44	36.94	60.38	-7.90	
	4EY6	73.84	46.51	37.30	59.93	-7.95	
Alpha-esterase-7	5TYJ	65.77	41.39	29.66	56.57	-7.15	7
	5TYP	66.55	37.93	31.37	56.31	-7.20	
Beta-*N*-acetyl-D-hexosaminidase OfHex1	3OZP	66.98	49.25	27.99	63.57	-6.95	3
	3NSN	73.67	53.49	31.44	66.46	-6.60	
Chitinases	3WQV	71.25	45.80	31.75	59.25	-7.50	4
	3WL1	68.22	46.81	31.17	57.50	-7.50	
Ecdysone receptor (EcR)	1R1K	72.29	33.81	34.31	59.55	-8.25	5
	1R20	72.29	33.88	29.47	58.25	-7.45	
N-Acetylglucosamine-1-phosphate uridyltransferase (GlmU)	2V0K	65.00	26.87	22.88	55.46	-6.60	13
	2VD4	52.66	26.33	22.26	44.01	-5.75	
Octopamine receptor	4N7C	63.28	41.41	37.01	61.73	-6.00	8
Odorant Binding Protein	2GTE	71.79	41.11	35.63	65.89	-7.25	1
	3K1E	86.48	45.86	38.87	64.12	-6.15	
	5V13	86.99	48.81	38.97	61.75	-8.85	
	3N7H	74.66	38.05	32.27	60.13	-6.95	
Peptide deformylase	5CY8	71.69	34.42	26.22	62.32	-7.40	6
p-Hydroxyphenylpyruvate dioxygenase	6ISD	59.19	35.73	27.24	49.65	-7.05	11
Polyphenol oxidase (PPO)	3HHS	69.69	37.78	31.18	58.79	-6.20	9
Sterol carrier protein-2 (HaSCP-2)	4UEI	65.86	34.79	31.40	48.96	-7.30	10
Voltage-gated sodium channel	6A95	63.49	29.10	23.53	53.68	-6.75	12

2.4. Molecular dynamics simulations and free energy calculations results

MD simulations were performed in the protein ligand complexes to validate the IVS results, evaluate the flexibility and the interactions formed between compounds **3c** and **3g** with the two most probable targets predicted: OBP1 and AChE. The structure with the best score of these two groups was selected, 3K1E for OBP1 and 1QON for AChE. Parameters such as RMSD, solvent accessible surface area (SASA) and number of hydrogen bonds were calculated and are depicted in Table 2.

Overall, all the complexes and ligands present a low RMSD value, indicating that the systems are well equilibrated and stable. The complexes formed between OBP and compounds **3c** and **3g** show a lower RMSD than complexes formed with AChE (average of 2.1 Å versus 3.1 - 3.5 Å, respectively - Figure S2). This may indicate that compounds cause a higher degree of destabilization when in complex with AChE, particularly compound **3g**.

The compounds are buried deep into the pocket of both OBP1 and AChE, with a percentage of Potential Ligand SASA buried values above 90% and a low ligand SASA (Figure S3). This indicates that compound **3c** when in complex with OBP1 and AChE is

Preprints (www.preprints.org) | NOT PEER-REVIEWED | Posted: 28 March 2022 doi:10.20944/preprints202203.0354.v1

very protected from the solvent and well bound to the proteins, throughout the simulations. Compound **3g** is more exposed to the solvent when in complex with OBP1, mainly due to the exposure of an aromatic ring (as evidenced in Figure 2).

Hydrogen bond analysis allows the understanding of the interactions that occur between the compounds **3c** and **3g** and the possible targets throughout time. Globally, these compounds maintain 1-3 hydrogen bonds, on average, with OBP1 and AChE. Compounds **3c** and **3g** can form more hydrogen bonds with AChE than with OBP1, particularly compound **3g** (Figure S4).

Table 2 also summarizes the values for the Gibbs binding free energy of association calculated using MM/GBSA and highlights the three most important amino acid residues involved in the stabilization of the ligands. The average structure of the dominant cluster of the OBP1 and AChE in complex with compounds **3c** and **3g**, obtained from the analysis of the MD trajectory are displayed in Figures 2 and 3, respectively. These figures illustrate the details of the binding pocket and the interaction formed between the targets and compounds **3c** and **3g**.

Table 2. Average protein and ligand RMSD values (Å), average ligand SASA (Å), percentage of potential ligand SASA buried, average number of ligand-target hydrogen bonds obtained from the MD simulations. ΔG binding energy determined using MM/GBSA and per-residue decomposition, calculated for the last 90 ns of the simulation.

		Average RMSD of the com-plex (Å)	Average RMSD of the ligand (Å)	Ligand SASA (Å²)	Potential ligand SASA buried (%)	Average number Hbonds	ΔG_{bind} (kcal/mol)	Main contributors (kcal/mol)
OBP1	**3c**	2.1 ± 0.4	1.1 ± 0.2	29.4 ± 9.1	94	0.4 ± 0.5	-34.8 ± 0.1	Ala88 (-2.0 ± 0.6) Trp114 (-2.7 ± 0.4) Tyr122 (-1.8 ± 0.4)
	3g	2.1 ± 0.2	1.0 ± 0.3	44.6 ± 10.7	91	0.7 ± 0.6	-37.0 ± 0.2	Trp114 (-2.4 ± 0.7) Met91 (-2.3 ± 0.5) Leu76 (-1.6 ± 0.3)
AChE	**3c**	3.1 ± 0.2	1.4 ± 0.2	24.3 ± 12.3	95	0.5 ± 0.6	-29.2 ± 0.2	Trp83 (-1.5 ± 0.4) Tyr370 (-1.9 ± 1.1) His480 (-1.5 ± 0.6)
	3g	3.5 ± 0.4	1.6 ± 0.1	7.2 ± 3.8	99	1.8 ± 0.9	-47.1 ± 0.2	Tyr71 (-2.4 ± 1.0) Ser238 (-1.9 ± 0.4) Ala239 (-2.1 ± 0.3)

Analyzing the Gibbs binding free energy of association, compound **3c** seems to have a higher affinity toward OBP1 (-34.8 kcal/mol vs -29.2 kcal/mol, when in complex with AChE). The opposite is observed for compound **3g**, that exhibits a higher affinity toward AChE (-47.1 kcal/mol vs -37.0 kcal/mol, respectively).

OBP1 are a class of proteins present in the olfactory system and have key roles in the perception and transmission of odorant molecules toward the receptors sites. They have been gaining increased attention as insecticidal targets in the development of eco-friendly repellents. They are a large family of proteins but have two common features, their small size and presence of six cysteine-rich residues paired with three interlocked disulfide bridges [27-29] There is a PDB structure of an OBP of a bee in complex with eugenol [30] and if these two eugenol derivatives studied, are able to maintain or show increased volatility, it is highly probable that they can work as repellents.

As seen on Figure 2, compound **3c** is mainly stabilized by hydrophobic interactions with residues Ala88 (-2.0 ± 0.6 kcal/mol), Trp114 (-2.7 ± 0.4 kcal/mol) and Tyr122 (-1.8 ± 0.4 kcal/mol). Tyr122 is also able to stabilize compound **3c** through a hydrogen bond. Compound **3g** is stabilized by Trp114 (-2.4 ± 0.7 kcal/mol), Met91 (-2.3 ± 0.5 kcal/mol) and Leu76

Preprints (www.preprints.org) | NOT PEER-REVIEWED | Posted: 28 March 2022 doi:10.20944/preprints202203.0354.v1

(-1.6 ± 0.3 kcal/mol). Trp114 can also interact via π-π stacking the compound **3g** and Ala10 can also stabilize compound **3g** through the formation of a hydrogen bond.

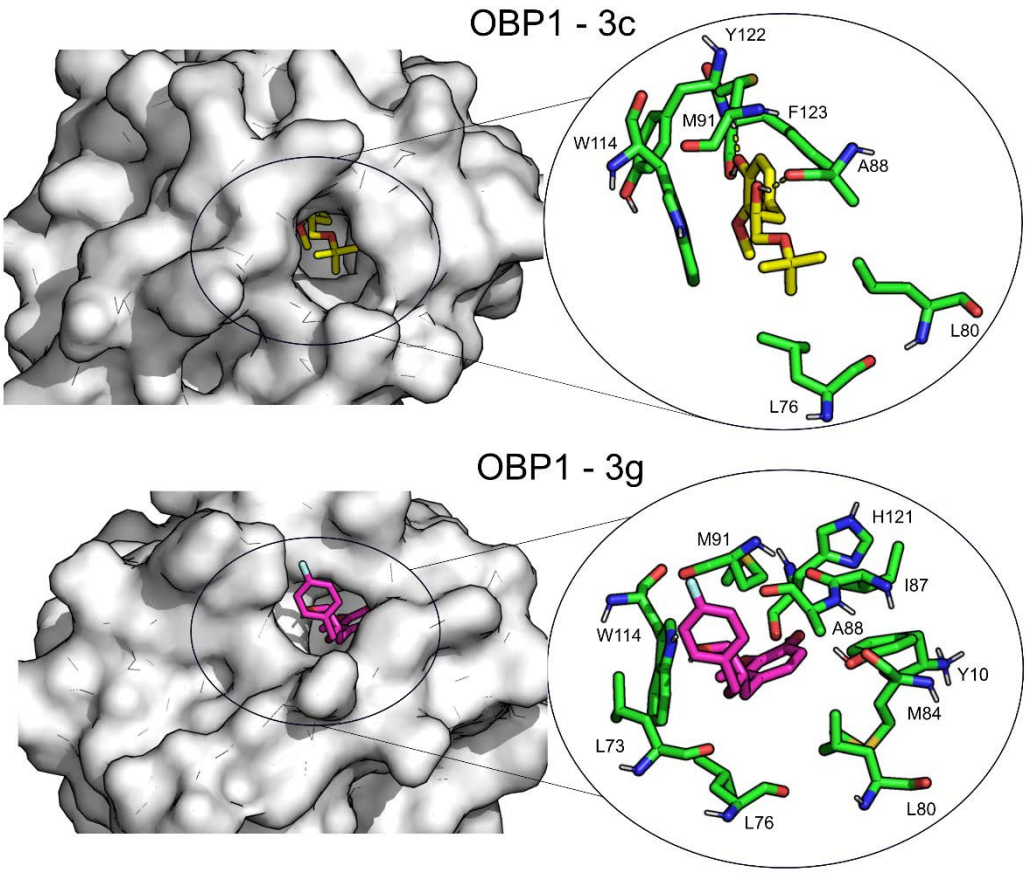

Figure 2. Compound **3c** (yellow licorice) and compound **3g** (magenta licorice) interaction map with OBP1. The most important residues for the interaction are highlighted in green. Hydrogen bond interactions are represented in yellow lines.

AChE is a very common target for insecticides because it is a key protein in the metabolism of acetylcholine in many different organisms, from mammals to insects. Due to the extensive use of insecticides that aim this serine hydrolase, many health and environmental problems arose. Moreover, insects were able to become resistant to these pesticides due to the mutation of the AChE gene. For these reasons, the search for new and more specific compounds able to block the mechanism of action of AChE is quite urgent [31-33].

Preprints (www.preprints.org) | NOT PEER-REVIEWED | Posted: 28 March 2022 doi:10.20944/preprints202203.0354.v1

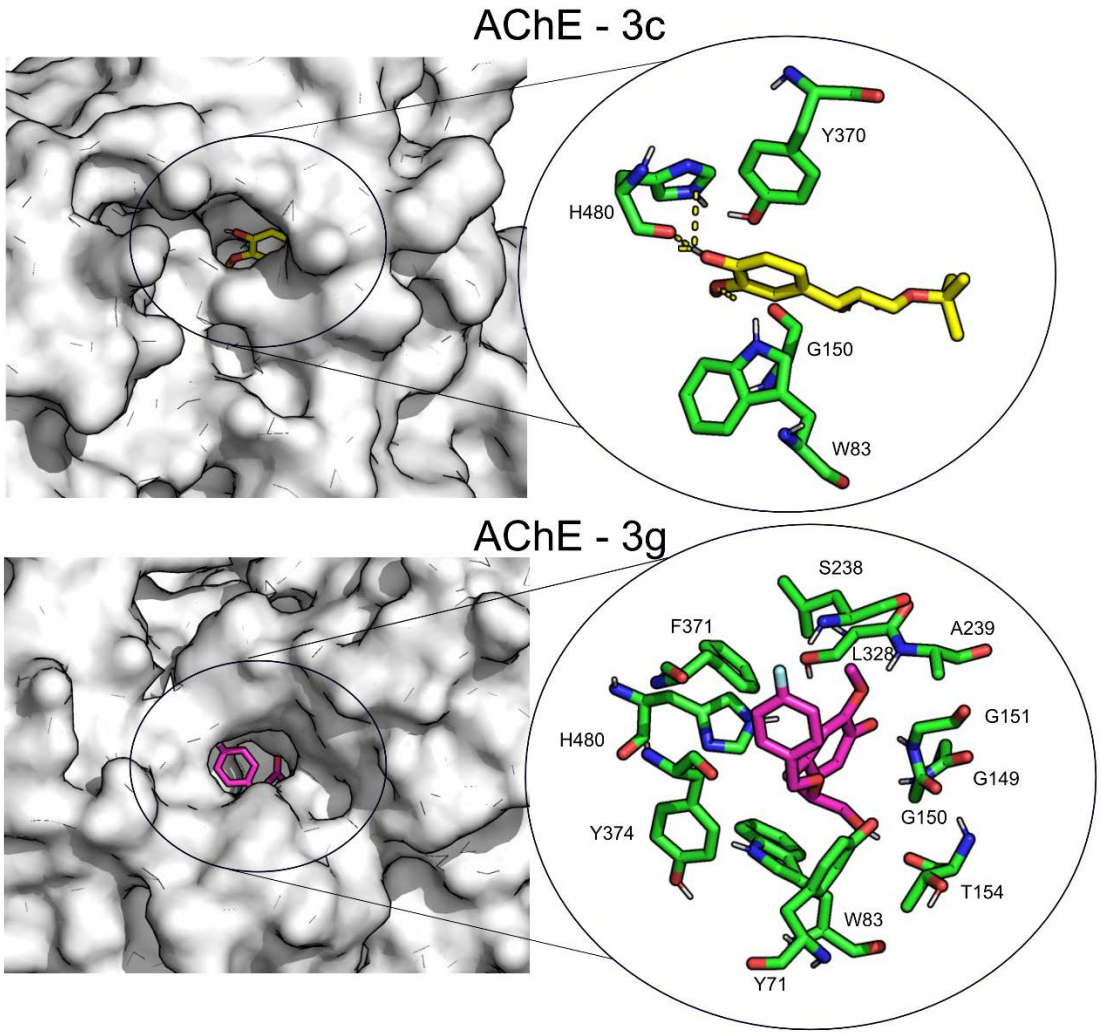

Figure 3. Compound **3c** (yellow licorice) and compound **3g** (magenta licorice) interaction map with AChE. The most important residues for the interaction are highlighted in green. Hydrogen bond interactions are represented in yellow lines.

As seen on Figure 3, compound **3c** is mainly stabilized through π-π stacking with Trp83 (-1.5 ± 0.4 kcal/mol), and Tyr370 (-1.9 ± 1.1 kcal/mol) and also through hydrogen bond formation with His480 (-1.5 ± 0.6 kcal/mol). Compound **3g** is stabilized through non-polar interactions, particularly with Tyr71 (-2.4 ± 1.0 kcal/mol), Ser238 (-1.9 ± 0.4 kcal/mol) and Ala239 (-2.1 ± 0.3 kcal/mol).

To access if compounds **3c** and **3g** could also bind to human AChE, a docking study was performed with a PDB structure of a human AChE (5HFA) and the scores were analyzed. The docking scores (Table S2) were inferior to the ones obtained for insect AChE, through most of the SF studied, indicating that there is a higher affinity toward this AChE sequence. This may be a starting point in the search for more specific pesticides.

2.5. Nanoencapsulation assays

The most active compounds against *Sf9* cells, compounds **3c** and **3g**, were encapsulated in Egg-PC:Ch (7:3) liposomes, prepared by two methods, ethanolic injection (EI) and thin Film hydration (TFH). EI is a very simple method and easy to scale-up, while TFH is more suitable for hydrophilic compounds than EI [34,35]. Hydrodynamic sizes, polydispersity (PDI) and zeta potential were measured by DLS (Table 3). The liposomes prepared by the EI method have a smaller size than the ones prepared by TFH, but both methods originate small polydispersity values. Considering the hydrodynamic size values, SUVs (Small Unilamellar Vesicles, with size around 100 nm) were formed through the EI

Preprints (www.preprints.org) | NOT PEER-REVIEWED | Posted: 28 March 2022 doi:10.20944/preprints202203.0354.v1

method, while MLVs (Multilamellar Vesicles, size around or below 500 nm) were originated by the TFH method. This result emphasizes the need of performing subsequent extrusion, to reduce the size of vesicles produced by TFH. Considering the zeta potential values, the liposomes obtained from both methods are considered neutral (zeta potential below ± 5 mV).

Table 3. Size (hydrodynamic diameter), polydispersity (PDI) and zeta potential of Egg-PC:Ch (7:3) liposomes determined by DLS. (SD: standard deviation from three independent measurements).

Method	Size ± SD (nm)	PDI ± SD	Zeta potential ± SD (mV)
EI	114.4 ± 1.8	0.27 ± 0.01	0.97 ± 0.3
TFH	484 ± 43	0.29 ± 0.02	3.03 ± 0.1

Taking advantage of the high sensitivity of fluorescence spectroscopy, the fluorescence emission of both compounds was used to determine the encapsulation efficiencies and to follow the release profile. Both compounds **3c** and **3g** revealed significant emission, with maximum wavelength around 340 nm, typical of simple aromatic moieties (Figure 4).

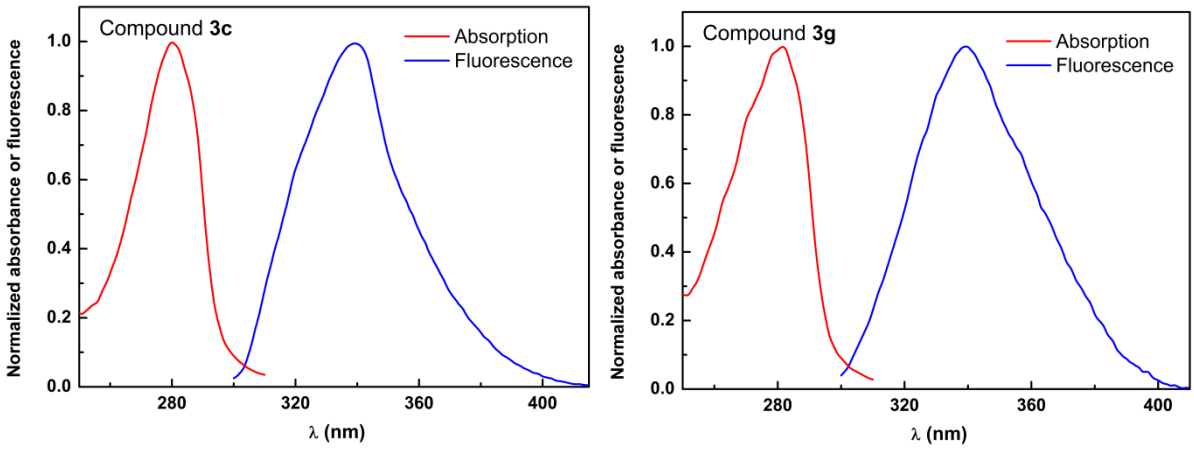

Figure 4. Normalized absorption and emission (λ_{exc}=290 nm) spectra of compounds **3c** (left) and **3g** (right) in ethanol.

Considering the encapsulation efficiencies, EE(%), determined by equation (1) (Table 4), both preparation methods have proven to be suitable for the two compounds, with very high EE(%) values, above 93%. However, the liposomes prepared by TFH method reveal higher EE(%) for both compounds **3c** and **3g**, with values of 96% and 99%, respectively.

Table 4. Encapsulation efficiency, EE(%), of compounds **3c** and **3g** in liposomes (SD: standard deviation of three independent measurements).

Compound	Method	EE(%) ± SD
3c	EI	93.5 ± 0.8
	TFH	96.0 ± 0.2
3g	EI	97.9 ± 0.6
	TFH	99.5 ± 0.2

The release of the encapsulated compounds **3c** and **3g** from the prepared liposomes of Egg-PC:Ch (7:3) was followed for 24 hours, at room temperature, towards buffer of pH = 7.4. The release is more effective for compound **3c** from liposomes prepared by thin film hydration, attaining *ca.* 60% in 24 hours. Both types of liposomes release less than 25% of encapsulated compound **3g** in 24 hours.

The release profiles were fitted to the Weibull and Korsmeyer-Peppas models (Figures 5 and 6, respectively). The fittings results to both methods are shown in Table 5.

Preprints (www.preprints.org) | NOT PEER-REVIEWED | Posted: 28 March 2022 doi:10.20944/preprints202203.0354.v1

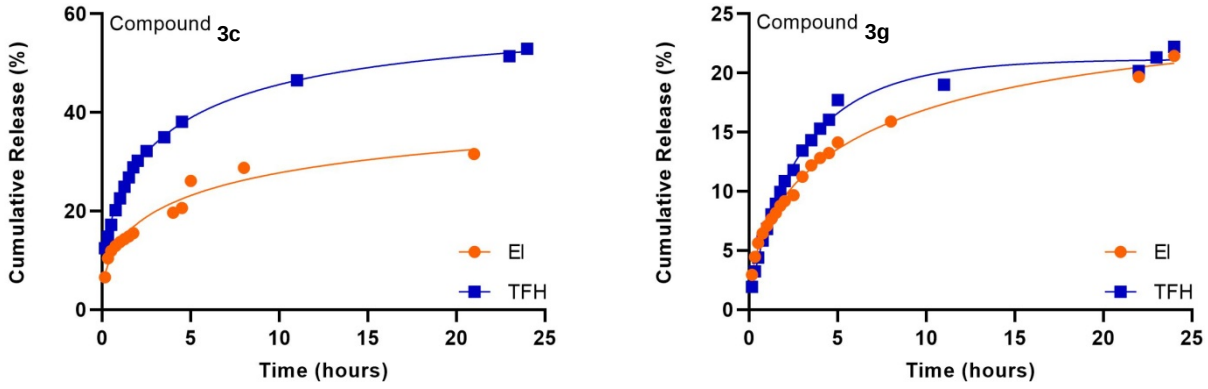

Figure 5. Release profiles of compounds **3c** (left) and **3g** (right) from liposomes of Egg-PC:Ch prepared by EI and TFH methods and fitting to Weibull model.

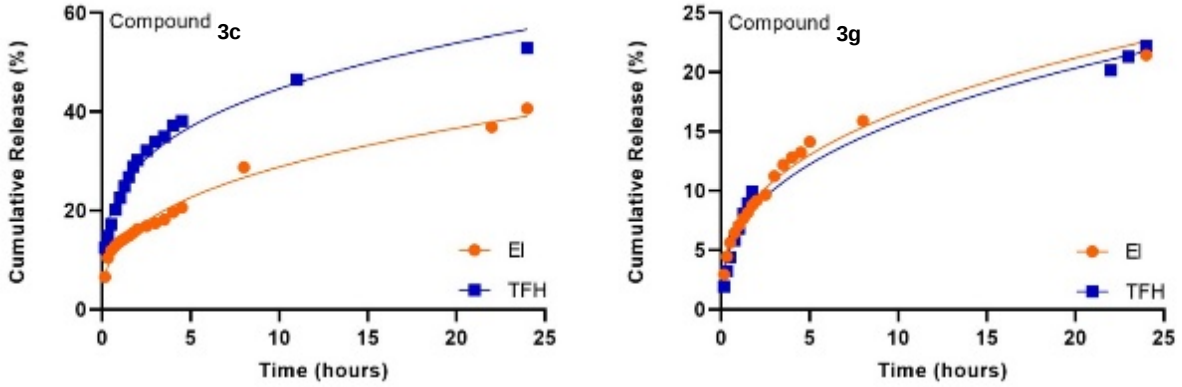

Figure 6. Release profiles of compounds **3c** (left) and **3g** (right) from liposomes of Egg-PC:Ch prepared by EI and TFH methods and fitting to Korsmeyer-Peppas model.

Table 5. Release parameters of the Weibull model (equation 2) and Korsmeyer-Peppas model fitted to the release profiles of compounds **3c** and **3g** from liposomes. R^2 is the coefficient of determination.

Compound	Method	Weibull				Korsmeyer-Peppas		
		Y_{max}	b	a	R^2	k (min^{-1})	n	R^2
3c	EI	41.65	0.44	0.40	0.96	12.94	0.35	0.98
	TFH	57.49	0.48	0.52	0.99	23.85	0.27	0.97
3g	EI	24.90	0.53	0.34	0.99	7.40	0.35	0.98
	TFH	21.19	0.83	0.40	0.99	6.78	0.37	0.98

The coefficients of determination (R^2) above 0.96 show that both Weibull and Korsmeyer-Peppas models are suitable to describe the release of compounds **3c** and **3g** from liposomes prepared by both methods. TFH method originates a faster compound release in the first 5 hours.

In general, the Weibull model originates better fits, with the exception of the release of compound **3c** from liposomes prepared by ethanolic injection. As reported by Papadopoulou *et al.* [36], the parameter b can be related to the diffusion mechanism; accordingly, if $b > 1$, the compound transport follows a complex release mechanism; if $b \leq 0.75$, a Fickian diffusion (in either fractal or Euclidian spaces) occurs; and if $0.75 < b < 1$, the mechanism is a combination of Fickian diffusion and Case II transport. Thus, the release mechanism of compound **3c** from liposomes of both methods and of compound **3g** from liposomes obtained by EI is Fickian diffusion, while the release mechanism of compound **3g** from liposomes obtained by TFH is a combination of Fickian diffusion and Case II transport.

 doi:10.20944/preprints202203.0354.v1

Regarding the Korsmeyer-Peppas model, some experimental points had to be neglected (not considered in the fitting procedure) to obtain a high coefficient of determination. According to Wu *et al.* [37], the parameter n is directly related to the release mechanism of the compound: if $n > 1$, the release is controlled by swelling and material relaxation; $0.89 < n < 1$ indicates a relaxation-controlled mechanism; $0.45 < n < 0.89$ indicates a combination of diffusion and erosion in drug release (non-Fickian release); and when $n < 0.45$, the release mechanism is diffusion-controlled (Fickian release). Thus, according to the Korsmeyer-Peppas model, the release mechanism of compounds **3c** and **3g** is diffusion-controlled (Fickian release). Overall, these results show that Egg-PC/Ch liposomes are suitable for encapsulation and a sustained release of the compounds exhibiting insecticidal activity.

3. Conclusions

A series of alkoxy alcohols were prepared by reaction of eugenol epoxide with various aliphatic and aromatic alcohols. The obtained eugenol derivatives were screened for their toxicity towards *Sf9* cells, in comparison with the corresponding precursors, to evaluate their application as biopesticides. The two semisynthetic compounds that showed promising insecticidal activity in *Sf9* namely 4-(3-(*tert*-butoxy)-2-hydroxypropyl)-2-methoxyphenol **3c** and 4-(2-((4-fluorobenzyl)oxy)-3-hydroxypropyl)-2-methoxyphenol **3g** were subjected to encapsulation in lipid nanosystems and release studies, exhibiting very high encapsulation efficiencies and a sustained release profile.

The *in silico* studies suggest that these two molecules have particularly strong affinity to two targets associated with insecticide activity, namely the odorant binding protein 1 and acetylcholinesterases. Possible binding modes are suggested for these two molecules, opening the way for future rational optimization efforts.

4. Materials and Methods

4.1. Chemistry

Dichloromethane, ethyl acetate, light petroleum, cesium carbonate, *m*-chloroperbenzoic acid were purchased from Fisher Scientific (Geel, Belgium). Methanol, ethanol, *tert*-butanol, phenol, 3-butyn-2-ol, 3-bromopropan-1-ol, 4-fluorobenzyl alcohol and trypan blue were from Sigma-Aldrich (St. Louis, MO, USA). Anhydrous magnesium sulphate and acetic anhydride were a PanReac Applichem (Barcelona, Spain) products. Chloroform-*d* was performed by Eurisotop (Cambridge, England). TLC analyses were carried out on 0.25 mm thick precoated silica plates (Merck Fertigplatten Kieselgel 60F254) and spots were visualized under UV light. Chromatography on silica gel was carried out on Merck Kieselgel (230-240 mesh). IR spectra were determined on a BOMEM MB 104 spectrophotometer. Absorption spectra (200–700 nm) were obtained using a Shimadzu UV/2501 PC spectrophotometer. NMR spectra were obtained on a Bruker Avance III at an operating frequency of 400 MHz for ^{1}H NMR and 100.6 MHz for ^{13}C NMR using the solvent peak as internal reference at 25 ^{o}C. All chemical shifts are given in ppm using δ Me_4Si = 0 ppm as reference and J values are given in hertz. Assignments were made by comparison of chemical shifts, peak multiplicities and J values and were supported by spin decoupling-double resonance and bidimensional heteronuclear correlation techniques. High-resolution mass spectrometry analyses were performed at the "Centro de Apoyo Científico y Tecnológico a la Investigación (CACTI), Servicio de Determinación Estructural, Proteómica y Genómica", at University of Vigo, Spain.

Preprints (www.preprints.org) | NOT PEER-REVIEWED | Posted: 28 March 2022 doi:10.20944/preprints202203.0354.v1

4.1.1. Procedure for obtaining 4-allyl-2-methoxyphenol 1

The extraction of 4-allyl-2-methoxyphenol, eugenol **1** was made from *Syzygium aromaticum* (cloves) in a round-bottom flask containing distilled water (200 mL) and the cloves (21.415 g). Hydrodistillation assembly was performed, and the mixture was refluxed during 2 h. The distillate was extracted with DCM (3 × 150 mL), the organic phase was dried over anhydrous magnesium sulphate, and solvent evaporation under vacuum gave 4-allyl-2-methoxyphenol, eugenol, **1** as an off-white oil (14% yield of extraction). ^{1}H NMR δ_H ($CDCl_3$, 400 MHz): 6.89 (d, *J* = 8.8 Hz, 1H, H-6), 6.73-6.71 (m, 2H, H-3 and H-5), 6.03-5.96 (m, 1H, C*H*=CH_2), 5.60 (broad s, 1H, OH), 5.14-5.08 (m, 2H, CH=CH_2), 3.89 (s, 3H, OCH_3), 3.36 (d, *J* = 6.8 Hz, 2H, CH_2Ph) ppm.

4.1.2. Synthesis of 2-methoxy-4-(oxiran-2-ylmethyl)phenol 2

In a reaction flask containing 3-chloroperoxybenzoic acid (*m*-CPBA) (0.750 g, 4.35 mmol, 1 equiv) dissolved in DCM (10 mL) while stirring in an ice bath (at 0 ºC), 4-allyl-2-methoxy phenol **1** (0.500 g, 3 mmol, 1 equiv), dissolved in DCM (10 mL) was added, dropwise, following a known procedure [26]. After stirring for 1 hour, additional *m*-CPBA (0.750 g, 4.35 mmol, 1 equiv) was added, the reaction was kept stirring for 24 hours at room temperature, and its evolution was monitored by ^{1}H NMR ($CDCl_3$). To the final product, DCM (20 mL) and 10% sodium sulfite aqueous solution (2 × 20 mL) were added, and the organic phase was collected. The collected organic phase was washed with saturated aqueous solution of sodium hydrogen carbonate (2 × 20 mL). The organic phase was dried over anhydrous magnesium sulfate and the remaining solvent was evaporated. Compound **2** was obtained as a dark orange oil (0.337 g, 67% yield). R_f = 0.27 (DCM). ^{1}H NMR δ_H ($CDCl_3$, 400 MHz): 6.87 (d, *J* = 7.6 Hz, 1H, H-6), 6.77 (d, *J* = 2 Hz, 1H, H-3), 6.75 (dd, *J* = 8 Hz and 2 Hz, 1H, H-5), 5.54 (broad s, 1H, OH), 3.90 (s, 3H, OCH_3), 3.16-3.12 (m, 1H, C*H*-oxirane), 2.82-2.79 (m, 3H, CH_2Ph and CH_2-oxirane), 2.55 (dd, *J* = 4.8 Hz and 2.8 Hz ,1H, CH_2-oxirane) ppm. ^{13}C NMR δ_C ($CDCl_3$, 100.6 MHz): 146.46 (C-2), 144.39 (C-1), 129.03 (C-4), 121.64 (C-5), 114.32 (C-6), 111.54 (C-3), 55.90 (OCH_3), 52.67 (*C*H-oxirane), 46.79 (*C*H_2-oxirane), 38.37 (*C*H_2Ph) ppm.

4.1.3. General procedure for the synthesis of eugenol alkoxy alcohols derivatives 3a-g

After distilling the solvent, and drying the reaction flask (under a nitrogen atmosphere) containing compound **2** (1 equiv), the respective alcohol (5 mL) and boron trifluoride diethyl etherate (1 equiv) were added. The reaction mixture was left stirring under a nitrogen atmosphere, at 0 ºC (ice bath with sodium chloride), for 2 hours. The progress of the reaction was monitored by ^{1}H NMR ($CDCl_3$) and TLC (AcOEt/EP 1:1). The solvent and/or alcohol was evaporated, the reaction mixture was dissolved in DCM (5 mL) and distilled water (5 mL) was added. The organic phase was extracted with DCM (2 × 5 mL), dried over anhydrous magnesium sulfate and the remaining solvent was evaporated.

4.1.3.1. 4-(2-Hydroxy-3-methoxypropyl)-2-methoxyphenol 3a

Starting from compound **2** (0.131 g, 0.73 mmol) and using methanol (5 mL), compound **3a** was obtained as a thick yellow oil (0.089g, 68% yield). R_f = 0.30 (ethyl acetate/light petroleum 1:1). IR (DCM) ν_{max} = 3412, 2933, 1602, 1516, 1463, 1453, 1431, 1369, 1154, 1124, 1035, 964, 911, 733 cm^{-1}. ^{1}H NMR δ_H ($CDCl_3$, 400 MHz): 6.86 (d, *J* = 7.6 Hz, 1H, H-6), 6.75 (d, *J* = 1.6 Hz, 1H, H-3), 6.71 (dd, *J* = 8 Hz and 2 Hz, 1H, H-5), 4.01-3.96 (m, 1H, C*H*OH), 3.89 (s, 3H, OCH_3), 3.44-3.40 (m, 1H, CH_2O), 3.40 (s, 3H, OCH_3), 3.40-3.28 (m, 1H, CH_2O), 2.73 (d, *J* = 6.8 Hz, 2H, CH_2Ph) ppm. ^{13}C NMR δ_C ($CDCl_3$, 100.6 MHz): 146.46 (C-2), 144.24 (C-1), 129.66 (C-4), 121.93 (C-5), 114.34 (C-6), 111.80 (C-3), 75.94 (CH_2O), 71.37 (CHOH), 59.06 (OCH_3), 55.85 (OCH_3), 39.47 (*C*H_2Ph) ppm.

HRMS (ESI-TOF): calcd for $C_{11}H_{16}O_4$ [M^++H]: 213.1049; found 213.1050.

4.1.3.2. 4-(3-Ethoxy-2-hydroxypropyl)-2-methoxyphenol 3b

Preprints (www.preprints.org) | NOT PEER-REVIEWED | Posted: 28 March 2022 doi:10.20944/preprints202203.0354.v1

Starting from compound **2** (0.109 g, 0.60 mmol) and using ethanol (5 mL), compound **3b** was obtained as white solid (0.023 g, 21% yield). R_f = 0.37 (ethyl acetate/light petroleum 1:1). IR (DCM) ν_{max} = 3395, 3279, 3055, 2998, 2976, 2920, 2859, 1601,1522, 1462, 1441, 1375, 1310, 1267, 1216, 1159, 1106, 1087, 1069, 1037, 907, 740 cm^{-1}. ^1H NMR δ_H ($CDCl_3$, 400 MHz): 6.86 (d, *J* = 8 Hz, 1H, H-6), 6.76 (d, *J* = 1.6 Hz, 1H, H-3), 6.71 (dd, *J* = 7.6 Hz and 1.6 Hz, 1H, H-5), 5.56 (broad s, 1H, OH), 4.02-3.96 (m, 1H, C*H*OH), 3.88 (s, 3H, OCH_3), 3.57-3.50 (m, 2H, O*C*$H_2$$CH_3$), 3.45-3.30 (m, 2H, CH_2O), 2.73 (d, *J* = 6.8 Hz, 2H, C*H*$_2$Ph), 1.22 (t, *J* = 14 Hz, 3H, OCH_2C*H*$_3$) ppm. ^{13}C NMR δ_C ($CDCl_3$, 100.6 MHz): 146.44 (C-2), 144.20 (C-1), 129.77 (C-4), 121.94 (C-5), 114.31 (C-6), 111.80 (C-3), 73.78 (CH_2O), 71.45 (CHOH), 66.72 (OCH_2CH_3), 55.85 (OCH_3), 39.52 (*C*H_2Ph), 15.13 (OCH_2*C*H_3) ppm. HRMS (ESI-TOF): calcd for $C_{12}H_{18}O_4$ [M^++H]: 227.1205; found 227.1204.

4.1.3.3. 4-(3-(tert-Butoxy)-2-hydroxypropyl)-2-methoxyphenol 3c

Starting from compound **2** (0.149 g, 0.83 mmol) and using *tert*-butanol (5 mL), compound **3c** was obtained as yellowish transparent oil (0.018 g, 12% yield). R_f = 0.54 (ethyl acetate/light petroleum 1:1). IR (DCM) ν_{max} = 3381, 2972, 2929, 2872, 1736, 1601, 1517, 1464, 1451, 1430, 1365, 1312, 1269, 1237, 1155, 1122, 1077, 1035, 939, 911, 873, 842, 820, 801, 756, 738 cm^{-1}. ^1H NMR δ_H ($CDCl_3$, 400 MHz): 6.85 (d, *J* = 8 Hz, 1H, H-6), 6.77 (d, *J* = 1.6 Hz, 1H, H-3), 6.72 (dd, *J* = 8 Hz and 2 Hz, 1H, H-5), 5.53 (broad s, 1H, OH), 3.94-3.89 (m, 1H, C*H*OH), 3.88 (s, 3H, OCH_3), 3.38-3.24 (m, 2H, CH_2O), 2.73 (d, *J* = 7.2 Hz, 2H, C*H*$_2$Ph), 1.20 (s, 9H, $OC(CH_3)_3$) ppm.^{13}C NMR δ_C ($CDCl_3$, 100.6 MHz): 146.38 (C-2), 144.09 (C-1), 130.12 (C-4), 121.91 (C-5), 114.24 (C-6), 111.77 (C-3), 73.19 ($OC(CH_3)_3$), 71.79 (CHOH), 64.91 (CH_2O), 55.84 (OCH_3), 39.54 (*C*H_2Ph), 27.57 $OC(CH_3)_3$) ppm. HRMS (ESI-TOF): calcd for $C_{14}H_{22}O_4$ [M^++H]: 255.1519; found 255.1518.

4.1.3.4. 4-(2-Hydroxy-3-phenoxypropyl)-2-methoxyphenol 3d

Starting from compound **2** (0.255 g, 1.42 mmol) and using phenol (0.133 g, 1.41 mmol), compound **3d** was obtained as thick brown oil (0.108 g, 42% yield). R_f = 0.48 (ethyl acetate/light petroleum 1:1). IR (DCM) ν_{max} = 3421, 3059, 2937, 2844, 1728, 1598, 1587, 1515, 1493, 1464, 1453, 1431, 1366, 1270, 1237, 1171, 1154, 1124, 1034, 1079, 955, 915, 819, 796, 754, 737 cm^{-1}. ^1H NMR δ_H ($CDCl_3$, 400 MHz): 7.32-7.27 (m, 2H, H-3 O-Ph and H-5 O-Ph), 6.99-6.94 (m, 3H, H-4 O-Ph, H-2 O-Ph and H-6 O-Ph), 6.85 (d, *J* = 8 Hz, 1H, H-6), 6.75 (d, *J* = 2 Hz, 1H, H-5), 6.72 (d, *J* = 8 Hz and 2 Hz, 1H, H-3), 5.53 (broad s, 1H, OH), 4.55-4.49 (m, 1H, C*H*OH), 3.84 (s, 3H, OCH_3), 3.81-3.71 (m, 2H, C*H*$_2$OPh), 2.99 (dd, *J* = 14 Hz and 5.6 Hz, 1H, C*H*$_2$Ph), 2.90 (dd, *J* = 14 Hz and 7.2 Hz, 1H, C*H*$_2$Ph) ppm. ^{13}C NMR δ_C ($CDCl_3$, 100.6 MHz): 157.79 (C-1 O-Ph), 146.42 (C-2), 144.30 (C-1), 129.64 (C-3 O-Ph and C-5 O-Ph), 129.04 (C-4), 122.08 (C-5), 121.42 (C-4 O-Ph), 116.24 (C-2 O-Ph and C-6 O-Ph), 114.36 (C-6), 112.03 (C-3), 79.63 (CHOH), 63.55 (CH_2O), 55.89 (OCH_3), 36.33 (CH_2Ph) ppm. HRMS (ESI-TOF): calcd for $C_{16}H_{18}O_4$ [M^++H]: 275.1205; found 275.1206.

4.1.3.5. 4-(2-(But-3-yn-2-yloxy)-3-hydroxypropyl)-2-methoxyphenol 3e

Starting from compound **2** (0.195 g, 1.08 mmol) and using 3-butyn-2-ol (0.076 g, 1.08 mmol), compound **3e** was obtained as thick brown oil (0.015 g, 8% yield). R_f = 0.56 (ethyl acetate/light petroleum 1:1). IR (DCM) ν_{max} = 3425, 3287, 2936, 2360, 1721, 1603, 1515, 1464, 1452, 1431, 1370, 1326, 1271, 1237, 1210, 1154, 1123, 1098, 1034, 955, 859, 818, 795, 739 cm^{-1}. ^1H NMR δ_H ($CDCl_3$, 400 MHz): 6.85 (d, *J* = 8 Hz, 1H, H-6), 6.73-6.71 (m, 2H, H-5 and H-3), 5.52 (broad s, 1H, OH), 4.06-4.01 (m, 1H, O*C*H(CH_3)CCH), 3.89 (s, 3H, OCH_3), 3.88-3.84 (m, 1H, CHO), 3.70-3.52 (m, 2H, C*H*$_2$OH), 2.76 (dd, *J* = 13.6 Hz and 6.8 Hz, 1H, C*H*$_2$Ph), 2.68 (dd, *J* = 14 Hz and 6.4 Hz, 1H, C*H*$_2$Ph), 2.44 (d, *J* = 2 Hz, 1H, OCH(CH_3)CC*H*), 1.37 (d, *J* = 6.4 Hz, 3H, OCH(C*H*$_3$)CCH) ppm. ^{13}C NMR δ_C ($CDCl_3$, 100.6 MHz): 146.37 (C-2), 144.19 (C-1), 129.76 (C-4), 122.01 (C-5), 114.33 (C-6), 111.84 (C-3), 84.41 (OCH(CH_3)*C*CH), 80.33 (CHO), 72.97 (OCH(CH_3)CCH), 64.69 (O*C*H(CH_3)CCH), 64.54 (CH_2OH), 55.90 (OCH_3),

 doi:10.20944/preprints202203.0354.v1

37.13 (CH_2Ph), 22.34 (OCH(CH_3)CCH) ppm. HRMS (ESI-TOF): calcd for $C_{14}H_{18}O_4$ [M^++H]: 251.1205; found 251.1204

4.1.3.6.4-(2-(3-. Bromopropoxy)-3-hydroxypropyl)-2-methoxyphenol 3f

Starting from compound **2** (0.231 g, 1.28 mmol) and using 3-bromopropan-1-ol (0.178 g, 1.28 mmol), compound **3f** was obtained as thick brown oil (0.035 g, 15% yield). R_f = 0.33 (ethyl acetate/light petroleum 1:1). IR (DCM) ν_{max} = 3398, 2927, 2854, 2361, 1741, 1659, 1603, 1515, 1464, 1452, 1431, 1365, 1271, 1236, 1210, 1154, 1122, 1105, 1034, 936, 858, 815, 797, 737 cm^{-1}. ^1H NMR δ_H ($CDCl_3$, 400 MHz): 6.85 (d, *J* = 8.4 Hz, 1H, H-6), 6.73 (s, 1H, H-3), 6.70 (dd, *J* = 9 Hz and *J* = 2 Hz, 1H, H-5), 5.51 (broad s, 1H, OH), 3.90 (s, 3H, OCH_3), 3.73-3.42 (m, 7H, CHO, O$CH_2$$CH_2CH_2$Br and C$H_2$OH), 2.83 (dd, *J* = 14 Hz and 6.4 Hz, 1H, CH_2Ph), 2.70 (dd, *J* = 14 Hz and 6.8 Hz, 1H, CH_2Ph), 2.09-2.02 (m, 2H, O$CH_2$$CH_2$$CH_2$Br) ppm. ^{13}C NMR δ_C ($CDCl_3$, 100.6 MHz): 146.46 (C-2), 144.14 (C-1), 129.87 (C-4), 121.99 (C-5), 114.29 (C-6), 111.83 (C-3), 81.62 (CHO), 67.02 (O$CH_2$$CH_2$$CH_2$Br), 63.67 ($CH_2$OH), 55.93 ($OCH_3$), 38.14 ($CH_2$Ph), 32.82 (O$CH_2$$CH_2$$CH_2$Br), 30.62 (O$CH_2$$CH_2$$CH_2$Br) ppm. HRMS (ESI-TOF): calcd for $C_{13}H_{19}BrO_4$ [M^++H]: 240.1284; found 240.1283.

4.1.3.7. 4-(2-((4-Fluorobenzyl)oxy)-3-hydroxypropyl)-2-methoxyphenol 3g

Starting from compound **2** (0.176 g, 0.98 mmol) and using 4-fluorobenzyl alcohol (0.123 g, 0.98 mmol), compound **3g** was obtained as thick brown oil (0.033 g, 19% yield). R_f = 0.42 (ethyl acetate/light petroleum 1:1). IR (DCM) ν_{max} = 3416, 3054, 2936, 2874, 1603, 1513, 1464, 1452, 1431, 1366, 1270, 1222, 1155, 1123, 1099, 1035, 853, 824, 737 cm^{-1}. ^1H NMR δ_H ($CDCl_3$, 400 MHz): 7.26-7.21 (m, 2H, H-2 *p*-F-Ph and H-6 *p*-F-Ph), 7.04-6.99 (m, 2H, H-5 *p*-F-Ph and H-3 *p*-F-Ph), 6.85 (d, *J* = 8 Hz, 1H, H-6), 6.72-6.69 (m, 2H, H-5 and H-3), 5.55 (broad s, 1H, OH), 4.49 (s, 2H, OCH_2-*p*-F-Ph), 3.84 (s, 3H, OCH_3), 3.71-3.48 (m, 1H, CH_2OH), 3.60-3.49 (m, 2H, CH_2OH and CHO), 2.85 (dd, *J* = 13.6 Hz and 6.8 Hz, 1H, CH_2Ph), 2.75 (dd, *J* = 14 Hz and 6.4 Hz, 1H, CH_2Ph) ppm. ^{13}C NMR δ_C ($CDCl_3$, 100.6 MHz): 161.13 (C-4 *p*-F-Ph), 146.38 (C-2), 144.17 (C-1), 133.99 (C-1 *p*-F-Ph) 129.86 (C-4), 129.57 (C-2 *p*-F-Ph), 129.49 (C-6 *p*-F-Ph), 122.00 (C-5), 115.37 (C-5 *p*-F-Ph), 115.16 (C-3 *p*-F-Ph), 114.30 (C-6), 111.91 (C-3), 80.98 (CHO), 71.27 (OCH_2-*p*-F-Ph), 63.80 (CH_2OH), 55.83 (OCH_3), 37.18 (CH_2Ph) ppm. HRMS (ESI-TOF): calcd for $C_{17}H_{19}FO_4$ [M^++H]: 307.1268; found 307.1267.

4.2. Cell Culture

Grace's insect medium, fetal bovine serum (FBS), penicillin/streptomycin solution (penicillin 10000 Units/mL and streptomycin 10000 µg/mL) and PrestoBlue™ were obtained from Invitrogen (Grand Island, NE, USA).

Insect cells (*Sf9*, *Spodoptera frugiperda*) were maintained as a suspension culture and cultivated in Grace's medium with 10% FBS and 1% penicillin/streptomycin, at 28 °C with agitation. Cells were used in experiments while in the exponential phase of growth.

4.3. Cell viability

For the assessment of viability, a resazurin-based method was used. The *Sf9* cells were plated at a density of 3.0×10^4, incubated for 24 h, and then exposed to the molecules under study (at 100 µg/mL in Grace's medium) for 24 h. After this period, a commercial solution of resazurin was added (1:10), and cells were incubated during 60 min, the kinetic reaction of fluorescence increase being then monitored at 560/590 nm (excitation/emission wavelength).

4.4. Inverted virtual screening studies

Inverted virtual screening (IVS) was the methodology used to identify possible targets for the eugenol alkoxy alcohols. In this strategy, a docking program is used to screen a collection of possible binding targets. In order to create a representative dataset of possible insecticide targets, Scopus was screened for studies that showed virtual screening

 doi:10.20944/preprints202203.0354.v1

(VS) studies involving targets and molecules with insecticidal activity using the keywords: "virtual screening" and "insecticide". The year of publication and relevance of target were the selection criteria, and the final list of potential targets identified 23 PDB structures. These are listed in Table S1

All the PDB structures were prepared for IVS using pymol [38] and the crystallographic ligands were saved in separate files to be used as reference to validate the binding pocket coordinates. In the absence of crystallographic ligands, the pocket coordinates were accessed based on the most relevant amino acid residues described in the literature. To validate and optimize the docking protocol, re-docking was used. Re-docking evaluates the ability of the docking software in reproducing the orientation and geometry of the ligand by comparing the docking prediction with the crystallographic structure of a target-ligand complex. The goal is to have the lowest root mean square deviation (RMSD) between the predicted pose and the reference position in the crystallographic structure.

Five docking scoring function alternatives were used: PLP, ASP, ChemScore, GoldScore (part of the GOLD software [39]) and AutoDock Vina [40] and the docking conditions were optimized for each of them to ensure consistency. The optimized parameters were: docking coordinates and box dimension (or radius in the case of GOLD), number of runs and exhaustiveness or search efficiency. The final and optimized protocol was then applied in the IVS stage. The chemical structure of the two eugenol derivatives studied (compounds **3c** and **3g**) were prepared using Datawarrior [41] and OpenBabel [42]. After docking these compounds into each PDB structure with the optimized conditions, for all the SF studied, a ranked list of the most probable targets was created, based on the average scores.

This protocol is well established and has been applied to other IVS studies involving eugenol and carvacrol derivatives [26,43].

4.5. Molecular dynamics simulations and free energy calculations

To evaluate and confirm the docking projections, molecular dynamics simulations (MD) was performed for compounds **3c** and **3g** bound to the most promising targets predicted (odorant binding protein 1 – PDB: 3K1E and acetylcholinesterase – PDB:1QON). Because there were gaps in the PDB structure of 1QON, a homology model was created using 50 of a total of 1466 templates obtained by SWISSMODEL [44] (Figure S1).

The ligand poses predicted in the IVS stage with GOLD/PLP were used for the MD simulations and treated with the Leap module of AMBER [45]. 1QON and 3K1E proteins were treated with the ff14SB force field [46] and the eugenol derivatives were parameterized using ANTECHAMBER, with the General Amber Force Field (GAFF) [47] and the RESP HF/6-31G(d) charges calculated with Gaussian16 [48]. The protein-ligand complexes were placed in TIP3P water boxes were with 12 Å distance between the surface of the protein and the side of the box. To neutralize the overall charge of the system, sodium (Na^+) counter ions were added.

Four minimization steps were performed to remove clashes, followed by two equilibration steps and a final 100 ns production step. The four consecutive minimization stages were applied in the following order: 1-water molecules (2500 steps); 2-hydrogens atoms (2500 steps); 3-side chains of all the amino acid residues (2500 steps); 4-full system (10000 steps). The equilibration procedure was divided in two stages: NVT ensemble, where the systems were heated to 298 K applying a Langevin thermostat at constant volume (50 ps); in the second stage, the density of the systems was further equilibrated at 298 K (subsequent 50 ps). The production run was performed using an NPT ensemble at constant temperature (298 K), pressure (1 bar, Berendsen barostat) and periodic boundary conditions. The SHAKE algorithm and an integration time of 2 fs was used, with a cut-off of 10 Å for nonbonded interactions. The resulting trajectories were analyzed using the cpptraj tool [49] of AMBER and VMD [50]. Parameters such as RMSD, number of hydrogen bonds formed, and accessible surface area were measured to evaluate the stability of the protein-

 doi:10.20944/preprints202203.0354.v1

ligand complexes. This overall procedure has been previously used with success in the treatment of several biomolecular systems [51-59].

To estimate the binding free energies of compounds **3c** and **3g** in complex with the odorant binding protein 1 and to acetylcholinesterase, the Molecular Mechanics - Generalized Born Surface Area (MM-GBSA) method [60] was applied, with a salt concentration of 0.100 mol.dm^{-3}. To estimate the contribution of the amino acid residues, the energy decomposition method was employed to each complex. From each MD trajectory, a total of 1400 conformations taken from the last 70 ns of simulation were considered for the MM-GBSA calculations.

4.6. Nanoencapsulation assays

Liposomal structures were prepared by both the ethanolic injection (EI) and thin film hydration (TFH) methods, using a lipid mixture of Egg-PC:Ch in the ratio 7:3, with a total lipid concentration of 1×10^{-3} M. In the EI method [34], the liposomes were prepared by a slow injection of an ethanolic solution of lipids and compound mixture to an aqueous buffer solution under vortexing. For TFH method [35], a lipid film of the Egg-PC:Ch mixture was obtained from the evaporation of a lipid solution in chloroform under an ultrapure nitrogen stream. The compound solution was added, and, after evaporation, the film was hydrated with the aqueous buffer solution, followed by bath sonication and vortexing.

For size (hydrodynamic diameter) and zeta potential measurements of compound-loaded liposomal formulations, three independent measurements (at 25 °C) were performed for each sample of liposomes obtained by the two different methods. A Dynamic Light Scattering (DLS) equipment, Litesizer 500 from Anton Paar, with a solid-state laser of 648 nm and 40 mW, was used for these measurements.

The encapsulation efficiency (percent), *EE%*, was determined through fluorescence measurements. After preparation, liposomes were subjected to centrifugation in Amicon® Ultra centrifugal filter units 100 kDa. at 11,000 rpm for 60 min. Then, the supernatant was removed and its fluorescence spectrum was measured in a Jobin-Yvon Fluorolog 3 spectrofluorometer. Using a previously obtained calibration curve of fluorescence intensity *versus* concentration, the encapsulation efficiencies of both compounds were determined through equation (1), and three independent assays were performed.

$$EE(\%) = \frac{Total\ quantity - Quantity\ of\ nonencapsulated\ compound}{Total\ quantity} \times 100 \qquad (1)$$

Release assays to phosphate buffer (pH = 7.4) were performed during 24 h, using Amicon® Ultra centrifugal filter units 100 kDa as dialysis membranes. The loaded liposomes solutions were maintained at 25 °C and were kept covered. The Weibull model was used to study the transport mechanism in compound release, being used for the comparison of release profiles from matrix systems. For that, the compound fraction accumulated (m) in solution on time t was fitted to the Weibull model [36] (equation 2),

$$m = 1 - \exp\left[\frac{-(t - T_i)^b}{a}\right] \qquad (2)$$

where a is a scale parameter that defines the timescale of the process, T_i represents the latency time of the release process (often being zero), and b is a formal parameter that characterizes the type of curve ($b = 1$ is exponential; $b > 1$ is sigmoid, with ascendant curvature delimited by an inflection point; and $b < 1$ is parabolic, displaying high initial slope and a consistent exponential character).

The Korsmeyer-Peppas model was also used to describe the compound release kinetics from the liposomes through equation 3:

$$M_t / M_\infty = K \cdot t^n \qquad (3)$$

where M_t/M_∞ represents the fraction of release drug, K is the release constant, n the transport exponent (dimensionless) and t is the time. When $n < 0.45$, the release mechanism is diffusion-controlled (Fickian release), $0.45 < n < 0.89$ indicates a combination of diffusion and erosion drug release (non-Fickian release), $0.89 < n < 1$ indicates a relaxation-controlled release, and in the case of $n > 1$, the release is controlled by swelling and chain relaxation [61].

Acknowledgements: This research was funded by project PTDC/ASP-AGR/30154/2017 (POCI-01-0145-FEDER-030154) of the COMPETE 2020 program, co-financed by the FEDER and the European Union. The authors acknowledge also the Foundation for Science and Technology (FCT, Portugal) and FEDERCOMPETE-QREN-EU for financial support to the research centers CQ-UM (UID/QUI/00686/2021), CF-UM-UP (UIDB/04650/2021) and REQUIMTE (UIDB/50006/2020). Renato B. Pereira acknowledges PRIMA Foundation (H2020-PRIMA 2018—Section 2, Project MILKQUA) and FCT (PTDC/QUI-QFI/2870/2020) for the funding. The NMR spectrometer Bruker Avance III 400 is part of the National NMR Network and was purchased within the framework of the National Program for Scientific Re-equipment, contract REDE/1517/RMN/2005 with funds from POCI 2010 (FEDER) and FCT.

Conflicts of Interest: The authors declare no conflict of interest.

References

1. Dambolena JS, Zunino MP, Herrera JM, Pizzolitto RP, Areco VA, Zygadlo JA. Terpenes: natural products for controlling insects of importance to human health - A structure-activity relationship study. *Psyche A J Entomol.* 2016;2:1–17. http://dx.doi.org/10.1155/2016/4595823

2. Ayvaz A, Sagdic O, Karaborklu S, Ozturk I. Insecticidal Activity of the essential oils from different plants against three stored-product insects. *J Insect Sci.* 2010;10:1–13. https://doi.org/10.1673/031.010.2101

3. Mossa A-TH. Green pesticides: essential oils as biopesticides in insect-pest management. *J Environ Sci Technol.* 2016;9:354–378. 10.3923/jest.2016.354.378

4. Khater HF. Prospects of botanical biopesticides in insect pest management. *J Appl Pharm Sci.* 2012; 3:641–656. http://dx.doi.org/10.5567/pharmacologia.2012.641.656

5. Oliveira LH, Trigueiro P, Souza JSN, Carvalho MS, Osajima JA, Silva-Filho EC, Fonseca MG Montmorillonite with essential oils as antimicrobial agents, packaging, repellents, and insecticides: an overview. *Colloids Surf B.* 2022;*209*:112186. https://doi.org/10.1016/j.colsurfb.2021.112186

6. Spinozzi E, Maggi F, Bonacucina G, Pavela R, Boukouvala MC, Kavallieratos NG, Canale A, Romano D, Desneux N, Wilke ABB, Beier JC, Benelli G. Apiaceae essential oils and their constituents as insecticides against mosquitoes-A review. *Ind Crops Prod.* 2021;171:113892. https://doi.org/10.1016/j.indcrop.2021.113892

7. Koul O, Walia S, Dhaliwal GS. Essential oils as green pesticides: Potential and constraints. *Biopestic Int.* 2008;4:63–84.

8. Munda S, Pandey SK, Dutta S, Baruah J, Lal M. Antioxidant activity, antibacterial activity and chemical composition of essential oil of *artemisia vulgaris* L. Leaves from Northeast India. *J Essent Oil-Bear Plants.* 2019;22:368-379. 10.1080/0972060X.2019.1602083

9. Labiad MH, Belmaghraoui W, Ghanimi A, El-Guezzane C, Chahboun N, Harhar H, Egea-Gilabert C, Zarrouk A, Tabyaoui M. Biological properties and chemical profiling of essential oils of *Thymus* (*vulgaris, algeriensis* and *broussonettii*) grown in Morocco. *Chem Data Coll*. 2022;37:100797. https://doi.org/10.1016/j.cdc.2021.100797

10. Nollet LML, Rathore HS. Green pesticides handbook: essential oils for pest control. Boca Raton: Taylor & Francis, CRC Press, 2017. https://doi.org/10.1201/9781315153131

11. Isman MB. Pesticides based on plant essential oils: phytochemical and practical considerations. In: eds. Jeliazkov VD Cantrell CL, eds. *Medicinal and Aromatic Crops: Production, Phytochemistry, and Utilization* ACS Publications; 2016; 218:13–26.

12. Ju J, Xie Y, Yu H, Guo Y, Cheng Y, Qian H, Yao W. Analysis of the synergistic antifungal mechanism of eugenol and citral. *LWT*

Food Sci Technol. 2020;123:109128. 10.1016/j.lwt.2020.109128

13. Fonsêca DV, Salgado PR, Aragão Neto HC, Golzio AM, Caldas Filho MR, Melo CG, Leite FC, Piuvezam, MR, Pordeus LC, Barbosa Filho JM, Almeida RN. Ortho-eugenol exhibits anti-nociceptive and anti-inflammatory activities. *Int Immunopharmacol.* 2016;38:402-408. 10.1016/j.intimp.2016.06.005

14. Silva FFM, Monte FJQ, Lemos TLG, Nascimento PGG, Costa AKM, Paiva LMM. Eugenol derivatives: synthesis, characterization, and evaluation of antibacterial and antioxidant activities. *Chem Cent J.* 2018;12: 34-42. https://doi.org/10.1186/s13065-018-0407-4

15. Isac-García J, Dobado JA, Calvo-Flores FG, Martínez-García H. *Experimental Organic Chemistry: Laboratory Manual*. 2nd ed. Academic Press; London; 2016.

16. Xu H, XS Z, Yang Y, Tian J-C, YH L, Tan KH, Heong KL, Lu Z. Methyl eugenol bioactivities as a new potential botanical insecticide against major insect pests and their natural enemies on rice (Oriza sativa). *Crop Prot.* 2015;72:144–149. 10.1016/j.cropro.2015.03.017

17. Wang L, Zhang Y. Eugenol nanoemulsion stabilized with zein and sodium caseinate by self-assembly. *J Agric Food Chem.* 2017;*65*:2990–2998. 10.1021/acs.jafc.7b00194

18. Chen CH, Tung SH, Jeng RJ, Abu-Omar MM, Lin CH. A facile strategy to achieve fully bio-based epoxy thermosets from eugenol. *Green Chem.* 2019;21:4475–4488. https://doi.org/10.1039/C9GC01184F

19. Novato T, Gomes GA, Zeringóta V, Franco CT, de Oliveira DR, Melo D, de Carvalho, MG, Daemon E, de Oliveira Monteiro CM. In vitro assessment of the acaricidal activity of carvacrol, thymol, eugenol and their acetylated derivatives on Rhipicephalus microplus (Acari: Ixodidae). *Vet Parasitol*. 2018;*30*:1-4. 10.1016/j.vetpar.2018.07.009.

20. Bras JL, Chatterjee D, Muzart J. A simple one-pot synthesis of β-alkoxy alcohols from alkenes *Tetrahedron Lett.* 2005;*46*:4741–4743. 10.1016/j.tetlet.2005.05.030

21. Manjunathan P, Prasanna V, Shanbhag GV. Exploring tailor-made Brønsted acid sites in mesopores of tin oxide catalyst for β-alkoxy alcohol and amino alcohol syntheses. *Sci Rep.* 2021;11:15718. https://doi.org/10.1038/s41598-021-95089-1

22. Kahandal SS, Kale SR, Disale ST, Jayaram RV. Sulphated yttria-zirconia as a regioselective catalyst system for the alcoholysis of epoxides. *Catal Sci Technol.* 2012;2:1493–1499. https://doi.org/10.1039/C2CY20116J

23. Chakraborty TK, Chattopadhyay AK, Samanta R, Ampapathi RS. Stereoselective construction of quaternary chiral centers using Ti(III)-mediated opening of 2,3-epoxy alcohols: studies directed toward the synthesis of penifulvins. *Tetrahedron Lett.* 2010;*51*:4425–4428.

24. Azizi N, Saidi MR. Highly Chemoselective Addition of Amines to Epoxides in Water. *Org Lett.* 2005;7:3649–3651. https://doi.org/10.1021/ol051220q

25. Fernandes MJG, Pereira RB, Pereira DM, Fortes AG, Castanheira EMS, Gonçalves MST. New eugenol derivatives with enhanced insecticidal activity. *Int J Mol Sci.* 2020;21:9257.10.3390/ijms21239257

26. Pereira RB, Pinto NFS, Fernandes MJG, Vieira TF, Rodrigues ARO, Pereira DM, Sousa SF, Castanheira EMS, Fortes AG, Gonçalves MST. Amino alcohols from eugenol as potential semisynthetic insecticides: chemical, biological, and computational insights. *Molecules*. 2021;26:6616. https://doi.org/10.3390/molecules26216616

27. Ghavami MB, Khoeini S, Djadid ND. Molecular characteristics of odorant-binding protein 1 in Anopheles maculipennis. *Malar J.* 2020;19:29. https://doi.org/10.1186/s12936-019-3058-6

28. Brito NF, Moreira MF, Melo ACA. A look inside odorant-binding proteins in insect chemoreception. *J Insect Physiol.* 2016;95:51–65. 10.1016/j.jinsphys.2016.09.008

29. Brito NF, Oliveira DS, Santos TC, Moreira MF, Melo ACA. Current and potential biotechnological applications of odorant-binding proteins. *Appl Microbiol Biotechnol.* 2020;20: 8631–8648. 10.1007/s00253-020-10860-0

30. Spinelli S, Lagarde A, Iovinella I, Legrand P, Tegoni M, Pelosi P, Cambillau C. Crystal structure of Apis mellifera OBP14, a C-minus odorant-binding protein, and its complexes with odorant molecules. *Insect Biochem Mol Biol.* 2012;42:41–50. 10.1016/j.ibmb.2011.10.005

31. Harel M, Kryger G, Rosenberry TL, Mallender WD, Lewis TR, Fletcher J, Guss JM, Silman I, Sussman JL. Three-dimensional structures of Drosophila melanogaster acetylcholinesterase and of its complexes with two potent inhibitors. *Protein Sci.* 2000;9:1063–1072. 10.1110/ps.9.6.1063

32. Pang, Y-P, Brimijoin S, Ragsdale DW, Zhu KY, Suranyi R. Novel and viable acetylcholinesterase target site for developing effective and environmentally safe insecticides. *Curr Drug Targets*. 2012;13:471–482. 10.2174/138945012799499703

33. Lang, G-J, Zhu KY, Zhang C-X. Can acetylcholinesterase serve as a target for developing more selective insecticides? *Curr Drug Targets*. 2012;13:495–501. 10.2174/138945012799499712

34. Jaafar-Maalej C, Diab R, Andrieu V, Elaissari A, Fessi H. Ethanol injection method for hydrophilic and lipophilic drug-loaded liposome preparation. *J Liposome Res.* 2010;20:228–243. 10.3109/08982100903347923

35. Zhang, H. Thin-film hydration followed by xxtrusion method for liposome preparation. In: D'Souza GG M, ed. *Liposomes: methods and protocols, methods in molecular biology*. 2017;1522:17–22. 10.1007/978-1-4939-6591-5_2

36. Papadopoulou V, Kosmidis K. Vlachou M, Macheras P. On the use of the Weibull function for the discernment of drug release mechanisms. *Int J Pharm.* 2006;309:44-50. 10.1016/j.ijpharm.2005.10.044

37. Wu IY, Bala S, Škalko-Basnet N, di Cagno MP. Interpreting non-linear drug diffusion data: Utilizing Korsmeyer-Peppas model to study drug release from liposomes. *Eur J Pharm Sci.* 2019;138:105026. 10.1016/j.ejps.2019.10502638. Schrödinger, L. & DeLano, W., 2020. *PyMOL*, Available at: http://www.pymol.org/pymol.

39. Jain AN. Scoring Functions for Protein-Ligand Docking. Curr Protein Pept Sci. 2006;7:407–420. 10.2174/138920306778559395

40. O. Trott and A. J. Olson, "AutoDock Vina: Improving the speed and accuracy of docking with a new scoring function, efficient optimization, and multithreading," *J. Comput. Chem.*, vol. 31, no. 2, p. NA-NA, 2009. 10.1002/jcc.21334

41.Sander T, Freyss, J, von Korff, M, Rufener C. DataWarrior: An open-source program for chemistry aware data visualization and analysis. *J Chem Inf Model.* 2015;55,460–473. https://doi.org/10.1021/ci500588j.

42. O'Boyle NM, Banck M, James CA, Morley C, Vandermeersch T, Hutchison, GR. Open Babel: An open chemical toolbox. *J Cheminform.* 2011;3:33. 10.1186/1758-2946-3-33

43. Natal CM, Fernandes, MJG, Pinto NFS, Pereira RB, Vieira TF, Rodrigues ARO, Pereira DM, Sousa SF, Fortes AG, Castanheira EMS, Gonçalves, MST. New carvacrol and thymol derivatives as potential insecticides: synthesis, biological activity, computational studies and nanoencapsulation. RSC Advances, 2021;11:34024-34035. 10.1039/D1RA05616F

44.Waterhouse A, Bertoni M, Bienert, S. Studer G, Tauriello G, Gumienny R, Heer FT, de Beer TAP, Rempfer C, Bordoli L, Lepore, Schwede T. SWISS-MODEL: homology modelling of protein structures and complexes. *Nucleic Acids Res.* 2018;46:296–303. https://doi.org/10.1093/nar/gky427

45. Wang J, Wolf RM, Caldwell JW, Kollman PA, Case DA. Development and testing of a general amber force field. *J Comput Chem.* 2004;25:1157-1174. https://doi.org/10.1002/jcc.20035

46. Maier JA, Martinez C, Kasavajhala K, Wickstrom L, Hauser KE, Simmerling C. ff14SB: Improving the accuracy of protein side chain and backbone parameters from ff99SB. *J. Chem. Theory Comput.* 2015;11:3696–3713. 10.1021/acs.jctc.5b00255

47. Wang J, Wang W, Kollman P, Case D. Automatic atom type and bond type perception in molecular mechanical calculations. *J. Mol Graphics Modell.* 2006;25:247–260. https://doi.org/10.1016/j.jmgm.2005.12.005

48. Frisch MJ *et al*., Gaussian 09, Revision A.02. Gaussian Inc., Wallingford CT, 2016.

49. Roe DR, Cheatham TE. PTRAJ and CPPTRAJ: Software for processing and analysis of molecular dynamics trajectory data. *J Chem Theory Comput.* 2013;9:3084–3095. 10.1021/ct400341p

50. Humphrey W, Dalke A, Schulten K. VMD: Visual molecular dynamics. *J Mol Graph.* 1996;14:33–38. 10.1016/0263-7855(96)00018-5

51. Lapaillerie D, Charlier C, Fernandes HS, Sousa SF, Lesbats P, Weigel P, Favereaux A, Guyonnet-Duperat V, Parissi V. In silico, in vitro and in cellulo models for monitoring SARS-CoV-2 Spike/Human ACE2 complex, viral entry and cell fusion. *Viruses.* 2021;3:365. https://doi.org/10.3390/v13030365

52. Martins FG, Melo A, Sousa SF. Identification of new potential inhibitors of quorum sensing through a specialized multi-level computational approach. *Molecules.* 2021;26:2600. https://doi.org/10.3390/molecules26092600

53. Moorthy NSHN, Sousa SF, Ramos MJ, Fernandes PA. Molecular dynamic simulations and structure-based pharmacophore development for farnesyltransferase inhibitors discovery. *J Enzyme Inhib Med Chem.* 2016;31:1428–1442. 10.3109/14756366.2016.1144593

54. Sousa SF, Cerqueira NMFSA, Brás N, Fernandes PA, Ramos MJ. Enzymatic "tricks": carboxylate shift and sulfur shift. *Int J Quantum Chem* 2014;114:1253–1256. https://doi.org/10.1021/ja067103n

55. Sousa SF, Coimbra JT, Paramos D, Pinto R, Guimarães RS, Teixeira V, Fernandes, PA, Ramos MJ. Molecular dynamics analysis of a series of 22 potential farnesyltransferase substrates containing a CaaX-motif. *J Mol Model.* 2013;19:673–688. 10.1007/s00894-012-1590-1

56. Marcial BL, Sousa SF, Barbosa IL, Dos Santos HF, Ramo M.J. Chemically modified tetracyclines as inhibitors of MMP-2 matrix metalloproteinase: a molecular and structural study. *J Phys Chem B*. 2012;116:13644–13654. https://doi.org/10.1021/jp3079748

57. Sousa SF, Fernandes PA, Ramos MJ. Molecular dynamics simulations on the critical states of the farnesyltransferase enzyme. *Bioorg Med Chem.* 2009;17:3369–3378. 10.1016/j.bmc.2009.03.055

58. Sousa SF, Fernandes PA, Ramos MJ. Enzyme flexibility and the catalytic mechanism of farnesyltransferase: targeting the relation. *J Phys Chem B.* 2008;112:8681–8691. https://doi.org/10.1021/jp711214j

59. Wang E, Sun H, Wang J, Wang Z, Liu H, Zhang JZH, Tingjun HT. End-point binding free energy calculation with MM/PBSA and MM/GBSA: strategies and applications in drug design. *Chem Rev* 2019;119:9478–9508. https://doi.org/10.1021/acs.chemrev.9b00055

60. Genheden S, Ryde U. The MM/PBSA and MM/GBSA methods to estimate ligand-binding affinities. *Expert Opin Drug Discov.* 2015;10:449–461. 10.1517/17460441.2015.1032936

61. Korsmeyer RW, Gurny R, Doelker E, Buri P, Peppas NA. Mechanisms of solute release from porous hydrophilic polymers. *Int J Pharm.* 1983;15:25-35. https://doi.org/10.1016/0378-5173(83)90064-9